Main-Chain Chiral Smectic Polymers Showing a Large Electroclinic Effect in the SmA* Phase

ARTICLE *in* CHEMISTRY OF MATERIALS · SEPTEMBER 2006

Impact Factor: 8.35 · DOI: 10.1021/cm0606373

9 AUTHORS, INCLUDING:

David M. Walba
University of Colorado Boulder
266 PUBLICATIONS **5,356** CITATIONS
SEE PROFILE

Hong Yang
Southeast University (China)
56 PUBLICATIONS **339** CITATIONS
SEE PROFILE

Renfan Shao
University of Colorado Boulder
91 PUBLICATIONS **1,809** CITATIONS
SEE PROFILE

Dave A Coleman
RealD, Inc.
36 PUBLICATIONS **769** CITATIONS
SEE PROFILE

Main-Chain Chiral Smectic Polymers Showing a Large Electroclinic Effect in the SmA* Phase

David M. Walba,*,† Hong Yang,† Richard K. Shoemaker,† Patrick Keller,†,‡ Renfan Shao,§ David A. Coleman,§ Christopher D. Jones,§ Michi Nakata,§ and Noel A. Clark§

Department of Chemistry and Biochemistry, 215 UCB, University of Colorado, Boulder, Colorado 80309-0215, Institut Curie-Section De Recherche, UMR 168 CNRS/IC, 11 Rue P. et M. Curie, Cedex5 75231, Paris, France, and Department of Physics, 390 UCB, University of Colorado, Boulder, Colorado 80309-0390

Received March 16, 2006. Revised Manuscript Received June 27, 2006

The synthesis and characterization of a main-chain smectic liquid-crystalline polymer system designed for development into electromechanical actuators is described. The chemical structure is chosen to provide a large electroclinic effect in the SmA* phase, with large concomitant layer shrinkage (a rare combination). The polymers are prepared by acyclic diene metathesis polymerization (ADMET) of liquid-crystalline α,ω-dienes. Oligomers with a degree of polymerization of ∼10−30 are obtained using Grubbs first-generation catalyst, while oligomers with a degree of polymerization of ∼200 are obtained using Grubbs second-generation catalyst. All polymer samples show the following phase sequence: I − SmA* − SmC* − Glass. X-ray analysis of polymer powder samples demonstrates the desired layer shrinkage at the SmA* − SmC* transition. The polymers form well-aligned fibers by pulling from the isotropic melt, and X-ray analysis of fibers in the SmA* phase shows that in the bulk of the fiber the layers are oriented perpendicular to the fiber axis, while at the surfaces there appears to be a thin sheath where the layers are parallel to the fiber/air interface. The desired layer shrinkage with tilt at the SmA* − SmC* transition in these fibers is seen as well, and in the SmC* phase the fibers exhibit an interesting conical chevron layer structure. Electro-optic investigation of aligned thin films of the polymer, prepared from quenched fiber glasses using a novel technique, exhibit a large electroclinic effect, with substantial degradation of alignment quality upon field-induced tilt. This degradation in alignment quality, coupled with the layer shrinkage at the SmA* − SmC* transition demonstrated by X-ray scattering, strongly suggests the desired layer shrinkage with electroclinic tilt is in fact occurring in the polymer films.

Introduction

Liquid-crystal (LC) polymers, and in particular LC elastomers,[1] have been found to exhibit thermomechanical[2] and photomechanical[3] effects of potential utility in many interesting "artificial muscle" applications. The electroclinic effect[4] in SmA* elastomers represents an attractive approach to highly desirable electromechanical actuators, and several recent studies have been directed toward realizing such materials (see below). In this approach, a SmA* elastomer is aligned and oriented such that application of an electric field parallel to the smectic layers causes director tilt about an axis parallel to the field, and concomitant layer shrinkage along the layer normal, as indicated in Figure 1. This layer shrinkage then couples with the macroscopic aspect ratio of the sample, causing contraction along the layer normal and expansion parallel to the layers. Such an effect could show very large stress, albeit with relatively small strain (perhaps 10%). Most importantly, fast response times in both contraction and extension are expected.

For this application, a large electroclinic coefficient (induced optic axis tilt per unit of applied field) and large saturation induced tilt are clearly desired. However, most SmA* materials with a large electroclinic coefficient and saturation tilt are of the de Vries type, where tilt of the optic axis is not strongly coupled with layer shrinkage.[5] Herein, we describe initial results in a project aimed at achieving an electroclinic-based actuator. Specifically, synthesis and some properties of a non-cross-linked main-chain SmA* polymer

* To whom correspondence should be addressed. E-mail: walba@colorado.edu.
† Department of Chemistry and Biochemistry, University of Colorado.
‡ Institut Curie-Section De Recherche, UMR 168 CNRS/IC.
§ Department of Physics, University of Colorado.

(1) Zentel, R. *Angew. Chem., Int. Ed. Engl.* **1989**, *28*, 1407−1415.
(2) (a) de Gennes, P. G. *C. R. Acad. Sci. Paris* **1975**, *281b*, 101−103. (b) de Gennes, P.-G. *C. R. Acad. Sci. Paris, Ser. IIB* **1997**, *324*, 343−348. (c) Hebert, M.; Kant, R.; deGennes, P. G. *J. Phys. I* **1997**, *7*, 909−919. (d) Thomsen, D. L.; Keller, P.; Naciri, J.; Pink, R.; Jeon, H.; Shenoy, D.; Ratna, B. R. *Macromolecules* **2001**, *34*, 5868−5875. (e) Buguin, A.; Li, M. H.; Silberzan, P.; Ladoux, B.; Keller, P. *J. Am. Chem. Soc.* **2006**, *128*, 1088−1089.
(3) (a) Li, M. H.; Keller, P.; Li, B.; Wang, X. G.; Brunet, M. *Adv. Mater.* **2003**, *15*, 569−572. (b) Yu, Y. L.; Nakano, M.; Ikeda, T. *Nature* **2003**, *425*, 145−145. (c) Yu, Y. L.; Ikeda, T. *Macromol. Chem. Phys.* **2005**, *206*, 1705−1708.
(4) Garoff, S.; Meyer, R. B. *Phys. Rev. Lett.* **1977**, *38*, 848−851.
(5) (a) de Vries, A.; Ekachai, A.; Spielberg, N. *Mol. Cryst. Liq. Cryst* **1979**, *49* (Lett.), 143−152. (b) de Vries, A. *Mol. Cryst. Liq. Cryst* **1979**, *49* (Lett.), 179−185. (c) de Vries, A. *Mol. Cryst. Liq. Cryst* **1977**, *41*, 27−31. (d) Clark, N. A.; Bellini, T.; Shao, R.-F.; Coleman, D.; Bardon, S.; Link, D. R.; Maclennan, J. E.; Chen, X.-H.; Wand, M. D.; Walba, D. M.; Rudquist, P.; Lagerwall, S. T. *Appl. Phys. Lett.* **2002**, *80*, 4097−4099. (e) Xue, J.; Walba, D. M. Ferroelectric liquid crystal devices using materials with a de Vries smectic A phase. U.S. Patent No. 6,870,163, Mar. 22, 2005. (f) Lagerwall, J. P. F.; Coleman, D.; Korblova, E. K.; Jones, C.; Shao, R.; Oton, J. M.; Walba, D. M.; Clark, N.; Giesselmann, F. *Liq. Cryst.* **2006**, *33*, 17−23.

10.1021/cm0606373 CCC: $33.50
Published on Web 08/26/2006

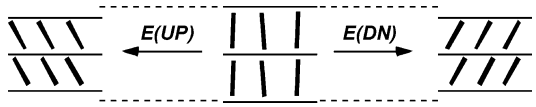

Figure 1. Illustration of the layer shrinkage accompanying electric field-induced director tilt (the electroclinic effect) in materials possessing a conventional SmA* phase. The system is chiral, and this hypothetical material shows positive induced polarization, defined as induced polarization being parallel to $z \times n$, where n is the "molecular director" and z is the layer normal.

system, designed to be the polymeric analogue of a low molar mass LC showing a rare combination of relatively large electroclinic coefficient and especially large electroclinic layer shrinkage, are described.

Experimental Section

General Considerations. For the mesogenic materials, liquid-crystal phases and phase transition temperatures were determined by polarized light microscopy using a Nicon-HCS400 microscope with an Instec-STC200 temperature-controlled stage. X-ray experiments were temperature-controlled with an Instec STC200 hotstage, and data were collected using a point detector mounted on a Huber four-circle goniometer at either of the following: Synchrotron radiation at beamline X10A of the National Synchrotron Light Source (NSLS), Brookhaven National Laboratory,[6] or Cu K(α) radiation from a Rigaku UltraX-18 rotating anode generator, operated by the Liquid Crystal Materials Research Center, University of Colorado-Boulder.

New compounds in the synthetic route were routinely characterized by NMR spectroscopy. ^{1}H NMR spectra were recorded at 500 or 400 MHz, using $CDCl_3$ (internal reference 7.24 ppm) as solvent. ^{13}C NMR spectra were obtained at 100 MHz using $CDCl_3$ (internal reference 77.23 ppm) as solvent. All nonaqueous reactions were conducted in oven-dried glassware, under a dry argon atmosphere. Grubbs Catalysts, first generation and second generation, were purchased from Aldrich. Chlorobenzene (99.8%) was purchased from Aldrich. CH_2Cl_2 was distilled from CaH_2 under nitrogen. THF was distilled from sodium-benzophenone ketyl under nitrogen. An IEC Centra CL2 centrifuge was used for isolation of the polymers after precipitation. All flash chromatography was performed using Sorbent Technologies 60 Å silica gel (32−63 μm).

Synthesis. Synthesis of the target polymers was accomplished as indicated in Scheme 1. Selective mononitration of biphenyl-4,4′-diol (**1**)[7] gave a mixture of the desired mono-nitro-biphenol **2**, along with dinitrated product (80:20), after chromatography of the crude product. This mixture was carried forward without separation of the nitrophenols.

Opening of the epoxide ring of unichiral epoxide **4** with the mixed cuprate derived from bromide **3** gave unichiral alcohol **5** in excellent yield. Regioselective Mitsunobu coupling of alcohol **5** with nitrophenol **2** gave the desired nitrophenol ether **9** in 76% yield, calculated based upon the 80% purity of the starting mononitrodiphenol.

Mitsunobu etherification[8] of methyl-*p*-hydroxybenzoate (**6**) with ω-hydroxy-decene (**7**), followed by hydrolysis of the resulting ester, gave acid **8**. Coupling of acid **8** with the phenolic nitroether **9** using the standard DCC/DMAP protocol then gave the mesogenic diene **10** in good yield.[9]

Scheme 1. Synthesis of the Main-Chain Smectic Mesogens

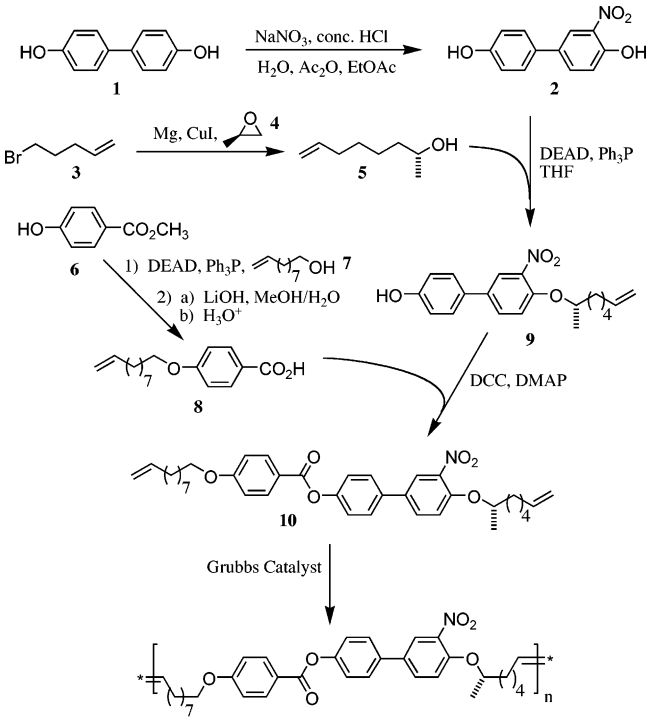

11a: n ~ 10. Glass - 40 °C - SmC* - 82 °C - SmA* - 130 °C - I
11a: n ~ 30. Glass - 45 °C - SmC* - 75 °C - SmA* - 130 °C - I
11b: n ~ 200. Glass - 51 °C - SmC* - 72 °C - SmA* - 130 °C - I

Diene **10** proved to be an excellent substrate for metathesis polymerization promoted by ruthenium alkylidene catalysts, to give polymers **11**. Polymers with degree of polymerization ranging from 10 to >200 could be obtained by variation of reaction conditions and catalyst (see Results and Discussion). Details of the synthesis are given below.

3-Nitro-biphenyl-4,4′-diol (2). Biphenyl-4,4′-diol (**1**) (10.0 g, 53.7 mmol) was dissolved in 500 mL of ethyl acetate. To the resulting solution was added $NaNO_3$ (5.0 g, 58.8 mmol) in 90 mL of H_2O solution. Acetic anhydride (0.5 mL) was then added. To this solution was added concentrated HCl (20.3 mL) dropwise. The two-phase reaction mixture was allowed to stir at room temperature for 2 h. Then, the layers were separated, and the aqueous layer was further extracted with ethyl acetate (3 × 200 mL). The combined organic layers were dried over anhydrous $MgSO_4$, filtered, and then concentrated at reduced pressure to give a black oil. Purification of this crude product by flash chromatography (5:1 hexanes:EtOAc) gave a mixture of 3-nitro-biphenyl-4,4′-diol and 3,3′-dinitro-biphenyl-4,4′-diol (80% and 20%, respectively, based upon ^{1}H NMR analysis) as a dark orange solid (11.46 g, 88.9%). This material was used in the subsequent reaction without further purification. ^{1}H NMR (500 MHz, $CDCl_3$): δ 10.53 (d, 1H, J = 6.00 Hz), 8.23 (d, 1H, J = 2.29 Hz), 7.76 (dd, 1H, J = 2.30, 8.70 Hz), 7.42 (AA′BB′, 2H), 7.35 (d, 1H, J = 8.69 Hz), 6.90 (AA′BB′, 2H). ^{13}C NMR (400 MHz, $CDCl_3$): δ 164.9, 152.9, 143.0, 134.1, 133.1, 131.8, 130.2, 128.7, 128.6, 120.7.

(*R*)-Oct-7-en-2-ol (5). A crystal of I_2 was added to predried Mg turnings (1.1 g, 45.26 mmol) under argon. A solution of 5-bromo-1-pentene (**3**) (6.54 g, 43.9 mmol) in 20 mL of dry THF was slowly added to the Mg under argon over a period of 2 h, which caused gentle refluxing of the solution. After completion of the addition, the mixture was allowed to stir for 1 h at 25 °C and 0.5 h at 0 °C. Solid CuI (fresh) (0.795 g, 2.37 mmol) was then added to the solution, which was allowed to stir for 0.5 h before slow addition of a solution of (*R*)-(+)-propylene oxide (**4**) (1.968 g, 33.88 mmol)

(6) Use of the National Synchrotron Light Source was supported by the U.S. Department of Energy, Office of Science, Office of Basic Energy Sciences, under Contract No. DE-AC02-98CH10886.
(7) Keller, P. *Bull. Soc. Chem. Fr.* **1994**, *131*, 27−29.
(8) Mitsunobu, O. *Synthesis* **1981**, 1−28.
(9) Neises, B.; Steglich, W. *Angew. Chem.* **1978**, *90*, 556−557.

in 12 mL of dry THF, keeping the temperature at 0 °C. The reaction mixture was allowed to stir for an additional 3 h at 0 °C, then poured into saturated NH_4Cl solution, stirred for 1 h, extracted with Et_2O, and dried with $MgSO_4$. Filtration and removal of solvent by rotary evaporation then gave an oil, which was directly subjected to purification by flash chromatography (4:1 hexanes−ethyl acetate) to provide (*R*)-oct-7-en-2-ol (**5**) (4.08 g, 94%) as a colorless oil. ^{1}H NMR (500 MHz, $CDCl_3$): δ 5.75−5.81 (m, 1H), 4.91−5.00 (m, 2H), 3.75−3.78 (m, 1H), 2.02−2.06 (m, 2H), 1.30−1.47 (m, 6H), 1.17 (d, 3H, J = 6.00 Hz). ^{13}C NMR (400 MHz, $CDCl_3$): δ 138.7, 114.2, 67.8, 40.0, 33.6, 28.8, 25.1, 23.3. Anal. Calcd for $C_8H_{16}O$: C, 74.94; H, 12.58. Found: C, 74.55; H, 12.55.

(*S*)-4′-(1-Methyl-hept-6-enyloxy)-3′-nitro-biphenyl-4-ol (9). Diethylazodicarboxylate (DEAD) (6.858 mL, 42.25 mmol) was added via syringe with stirring and under argon to a solution of a mixture of 3-nitro-biphenyl-4,4′-diol (**2**) and dinitro-diol prepared as described above (7.51 g total, containing 6.0 g, 25.0 mmol of **2** in admixture with dinitro-diol), (*R*)-oct-7-en-2-ol (**5**) (5.00 g, 39.0 mmol), and triphenyl phosphine (TPP) (11.2 g, 42.25 mmol) in 300 mL of dry THF. The reaction mixture was allowed to stir for 12 h at 25 °C and was then concentrated by rotary evaporation to give an orange oil which was directly subjected to purification by flash chromatography (20:1 hexanes−ethyl acetate) to provide (*S*)-4′-(1-methyl-hept-6-enyloxy)-3′-nitro-biphenyl-4-ol (**9**) (6.78 g, 76% based on nitrodiol **2**) as an orange oil. ^{1}H NMR (500 MHz, $CDCl_3$): δ 7.92 (d, 1H, J = 2.39 Hz), 7.62 (dd, 1H, J = 2.39, 8.71 Hz), 7.39 (AA′BB′, 2H), 7.07 (d, 1H, J = 8.89 Hz), 6.89 (AA′BB′, 2H), 5.77 (m, 1H), 5.18 (s, 1H), 4.96 (m, 2H), 4.50 (m, 1H), 2.04 (m, 2H), 1.78 (m, 1H), 1.63 (m, 1H), 1.41 (m, 4H), 1.35 (d, 3H, J = 6.13 Hz). ^{13}C NMR (400 MHz, $CDCl_3$): δ 155.7, 150.6, 141.2, 139.0, 133.4, 131.9, 131.5, 128.2, 123.6, 116.4, 116.2, 114.8, 76.7, 36.3, 33.8, 29.0, 25.0, 19.8. Anal. Calcd for $C_{20}H_{23}NO_4$: C, 70.36; H, 6.79; N, 4.10, Found: C, 70.35; H, 6.91; N, 4.08.

4-Dec-9-enyloxy-benzoic Acid. DEAD (3.90 mL, 24.0 mmol) was added via syringe with stirring and under argon to a solution of dec-9-en-1-ol (**7**) (3.75 mL, 21.0 mmol), 4-hydroxy-benzoic acid methyl ester (**6**) (3.07 g, 20.0 mmol), and TPP (6.49 g, 24.0 mmol) in 200 mL of dry THF. The reaction mixture was stirred for 12 h at 25 °C and then concentrated to an oil, which was directly subjected to purification by flash chromatography (10:1 hexanes−ethyl acetate) to provide 4-dec-9-enyloxy-benzoic acid methyl ester (5.08 g, 87%) as a white solid. ^{1}H NMR (500 MHz, $CDCl_3$): δ 7.96 (AA′BB′, 2H), 6.88 (AA′BB′, 2H), 5.79 (m, 1H), 4.94 (m, 2H), 3.98 (t, 2H, J = 6.50 Hz), 3.86 (s, 3H), 2.02, (m, 2H), 1.77 (m, 2H), 1.33 (m, 10H). ^{13}C NMR (400 MHz, $CDCl_3$): δ 167.2, 163.2, 139.4, 131.8, 122.5, 114.4, 114.3, 68.4, 52.1, 34.0, 29.6, 29.5, 29.3, 29.2, 29.1, 26.2. mp 36 °C (literature value: 36 °C).[10]

4-Dec-9-enyloxy-benzoic Acid (8). Lithium hydroxide monohydrate (2.17 g, 50.0 mmol) was added to a refluxing solution of 4-dec-9-enyloxy-benzoic acid methyl ester (1.50 g, 5.0 mmol) in 40 mL of methanol/H_2O (10/1 by volume). The reaction mixture was refluxed overnight and then was acidified with concentrated HCl to pH = 2. Water (200 mL) was added, and the solution was cooled. The resulting precipitated crude product was filtered, washed with water, and air-dried. Flash chromatography (3:1 hexanes−ethyl acetate) gave 4-dec-9-enyloxy-benzoic acid (**8**) (1.18 g, 83%) as a white solid. ^{1}H NMR (500 MHz, $CDCl_3$): δ 8.03 (AA′BB′, 2H), 6.91 (AA′BB′, 2H), 5.79 (m, 1H), 4.94 (m, 2H), 4.00 (t, 2H, J = 6.60 Hz), 2.02, (m, 2H), 1.79 (m, 2H), 1.34 (m, 10H). ^{13}C NMR (400 MHz, $CDCl_3$): δ 163.9, 139.4, 132.6, 121.6, 114.4, 68.5, 34.0, 29.6, 29.5, 29.3, 29.2, 29.1, 26.2. mp 54 °C (literature value: 54 °C).[10]

(*S*)-4-Dec-9-enyloxy-benzoic Acid 4′-(1-Methyl-hept-6-enyloxy)-3′-nitro-biphenyl-4-yl Ester (10). A solution of dicyclohexyl carbodiimide (DCC) (1.61 g, 7.71 mmol) in 10 mL of dry CH_2Cl_2 was added via syringe with stirring and under argon to a solution of (*S*)-4′-(1-methyl-hept-6-enyloxy)-3′-nitro-biphenyl-4-ol (**9**) (1.75 g, 5.14 mmol), 4-dec-9-enyloxy-benzoic acid (**8**) (1.70 g, 6.17 mmol), and DMAP (0.25 g, 2.06 mmol) in 40 mL of dry CH_2Cl_2. The reaction mixture was allowed to stir for 12 h at 25 °C and then concentrated by rotary evaporation to give crude product as an orange oil, which was directly subjected to purification by flash chromatography (20:1 hexanes−ethyl acetate) to provide 4-dec-9-enyloxy-benzoic acid (*S*)-4′-(1-methyl-hept-6-enyloxy)-3′-nitro-biphenyl-4-yl ester (**10**) (2.81 g, 91%) as a pale yellow oil. ^{1}H NMR (500 MHz, $CDCl_3$): δ 8.13 (AA′BB′, 2H), 7.98 (d, 1H, J = 2.42 Hz), 7.68 (dd, 1H, J = 2.42, 8.79 Hz), 7.57 (AA′BB′, 2H), 7.27 (AA′BB′, 2H), 7.11 (d, 1H, J = 9.01 Hz), 6.96 (AA′BB′, 2H), 5.79 (m, 2H), 4.94 (m, 4H), 4.53 (m, 1H), 4.03 (t, 2H, J = 6.60 Hz), 2.05 (m, 4H), 1.81 (m, 3H), 1.62 (m, 1H), 1.40 (m, 14H), 1.36 (d, 3H, J = 6.15 Hz). ^{13}C NMR (400 MHz, $CDCl_3$): δ 165.2, 163.9, 151.1, 151.0, 141.3, 139.4, 139.0, 136.4, 132.9, 132.6, 132.2, 128.0, 124.1, 122.7, 121.5, 116.3, 114.8, 114.6, 114.4, 76.7, 68.6, 36.3, 34.0, 33.8, 29.6, 29.5, 29.3, 29.2, 29.1, 29.0, 26.2, 25.0, 19.8. Anal. Calcd for $C_{37}H_{45}NO_6$: C, 74.10; H, 7.56; N, 2.34, Found: C, 74.23; H, 7.67; N, 2.46. Phase sequence and transition temperatures: SmA* − 54.5° − SmC* − I (on cooling, determined by polarized light microscopy).

Polymer 11a ($n \sim 10$). To a solution of (*S*)-4-dec-9-enyloxy-benzoic acid 4′-(1-methyl-hept-6-enyloxy)-3′-nitro-biphenyl-4-yl ester (**10**) (100 mg, 0.17 mmol) in 3 mL of dichloroethane was added benzylidene-bis(tricyclohexylphosphine)dichlororuthenium (Grubbs 1st generation catalyst) (1.5 mg, 0.002 mmol) under argon. The reaction was stirred under argon for 3 days. The resulting mixture was then concentrated by rotary evaporation to give a black oil. The crude product was redissolved in 3 mL of $CHCl_3$, and to this solution were added 2-propanol (1 mL) and tris(hydroxymethyl)phosphine (12.5 mg, 0.10 mmol) to remove traces of remaining catalyst.[11] The resulting solution was allowed to stir under argon at 55 °C for 24 h. The polymer product was then precipitated from the solution by addition of a large amount of methanol. The product was then separated from the solution by centrifugation, providing polymer **11a** ($n \sim 10$ by end group analysis using ^{1}H NMR) as a pale yellow powder (63 mg, 63%). ^{1}H NMR (500 MHz, $CDCl_3$): δ 8.13 (m), 7.98 (m), 7.68 (m), 7.57 (m), 7.27 (m), 7.11 (m), 6.96 (m), 5.30 (m), 4.59 (m), 4.03 (m), 2.05 (m), 1.81 (m), 1.62 (m), 1.40 (m). ^{13}C NMR (400 MHz, $CDCl_3$): δ 165.2, 163.9, 151.0, 141.3, 136.3, 132.9, 132.6, 132.2, 130.9, 130.6, 130.2, 128.0, 124.0, 122.7, 121.5, 116.3, 114.6, 76.7, 68.6, 36.3, 32.8, 32.6, 29.9, 29.6, 29.5, 29.3, 27.4, 26.2, 25.0, 19.8. Phase transitions: Glass − 40 °C − SmC* − 82 °C − SmA* − 130 °C − I (on cooling, determined by polarized light microscopy).

Polymer 11a ($n \sim 30$). To a solution of (*S*)-4-dec-9-enyloxy-benzoic acid 4′-(1-methyl-hept-6-enyloxy)-3′-nitro-biphenyl-4-yl ester (**10**) (100 mg, 0.17 mmol) in 3 mL of chlorobenzene was added benzylidene-bis(tricyclohexylphosphine)dichlororuthenium (Grubbs 1st generation catalyst) (1.5 mg, 0.002 mmol) under argon. The reaction system was connected to a dry vaccum pump (30 mmHg) for removal of ethene, and the reaction was allowed to proceed under vacuum for 1 day. The resulting mixture was then concentrated by rotary evaporation to give a black oil. The crude product was redissolved in 3 mL of $CHCl_3$, and to this solution were added 2-propanol (1 mL) and tris(hydroxymethyl)phosphine (12.5 mg, 0.10 mmol) to remove traces of remaining catalyst. The

(10) Medeiros, D. R.; Hale, M. A.; Hung, R. J. P.; Leitko, J. K.; Willson, C. G. *J. Mater. Chem.* **1999**, *9*, 1453−1460.

(11) Maynard, H. D.; Grubbs, R. H. *Tetrahedron Lett.* **1999**, *40*, 4137−4140.

resulting solution was allowed to stir under argon at 55 °C for 24 h. The polymer product was then precipitated from the solution by addition of a large amount of methanol. The product was then separated from the solution by centrifugation, providing polymer **11a** ($n \sim 30$ by end group analysis using ^{1}H NMR) as a pale yellow powder (63 mg, 63%). ^{1}H NMR (500 MHz, $CDCl_3$): δ 8.13 (m), 7.98 (m), 7.68 (m), 7.57 (m), 7.27 (m), 7.11 (m), 6.96 (m), 5.30 (m), 4.59 (m), 4.03 (m), 2.05 (m), 1.81 (m), 1.62 (m), 1.40 (m). ^{13}C NMR (400 MHz, $CDCl_3$): δ 165.2, 163.9, 151.0, 141.3, 136.3, 132.9, 132.6, 132.2, 130.9, 130.6, 130.2, 128.0, 124.0, 122.7, 121.5, 116.3, 114.6, 76.7, 68.6, 36.3, 32.8, 32.6, 29.9, 29.6, 29.5, 29.3, 27.4, 26.2, 25.0, 19.8. Phase transitions: Glass − 45 °C − SmC* − 75 °C − SmA* − 130 °C − I (on cooling, determined by polarized light microscopy).

Polymer 11b ($n \sim 200$). To a solution of 4-dec-9-enyloxybenzoic acid (*S*)-4′-(1-methyl-hept-6-enyloxy)-3′-nitro-biphenyl-4-yl ester (**10**) (400 mg, 0.67 mmol) in 7 mL of chlorobenzene was added benzylidene[1,3-bis(2,4,6-trimethylphenyl)-2-imidazolidinylidene]dichloro(tricycl ohexylphosphine)ruthenium (Grubbs 2nd generation catalyst) (5.5 mg, 0.007 mmol) under argon. The reaction system was connected to a dry vaccum pump (30 mmHg) for removal of ethene, and the reaction was allowed to proceed under vacuum for 3 days. The resulting mixture was then concentrated by rotary evaporation to give a black oil. The crude product was redissolved in 5 mL of $CHCl_3$, and to this solution were added 2-propanol (3 mL) and tris(hydroxymethyl)phosphine (50 mg, 0.40 mmol).[11] The resulting solution was allowed to stir under argon at 55 °C for 24 h. The polymer product was then precipitated from the solution by addition of a large amount of methanol. The product was then separated from the solution by centrifugation, providing polymer **11b** ($n > 200$ by DOSY) as a pale yellow powder (210 mg, 53%). ^{1}H NMR (500 MHz, $CDCl_3$): δ 8.13 (m), 7.98 (m), 7.68 (m), 7.57 (m), 7.27 (m), 7.11 (m), 6.96 (m), 5.30 (m), 4.59 (m), 4.03 (m), 2.05 (m), 1.81 (m), 1.62 (m), 1.40 (m). ^{13}C NMR (400 MHz, $CDCl_3$): δ 165.2, 163.9, 151.0, 141.3, 136.3, 132.9, 132.6, 132.2, 130.9, 130.6, 130.2, 128.0, 124.0, 122.7, 121.5, 116.3, 114.6, 76.7, 68.6, 36.3, 32.8, 32.6, 29.9, 29.6, 29.5, 29.3, 27.4, 26.2, 25.0, 19.8. Anal. Calcd for $C_{35}H_{41}NO_6$: C, 73.53; H, 7.23; N, 2.45, Found: C, 73.55; H, 7.41; N, 2.39. Phase transitions: Glass − 51 °C − SmC* − 72 °C − SmA* − 130 °C − I (on cooling, determined by polarized light microscopy).

Results and Discussion

Electroclinic Effect. The polymers presented here represent an initial step toward development of smectic elastomers showing an electromechanical effect with large stress and fast response. The choice of mesogen structure was made based upon the following considerations: (1) The presence of a chiral smectic A (SmA*) phase in the phase sequence; (2) a large electroclinic coefficient in the SmA* phase; and (3) substantial layer shrinkage concomitant with field-induced tilt of the optic axis.

Many interesting SmA* materials have been shown to exhibit optic axis tilts >10° upon application of an electric field parallel to the smectic layers. It is expected that this "optic axis tilt" of the director, θ_{opt}, should be accompanied by shrinkage of the smectic layers. It is customary in the tilted smectic field to refer to this layer shrinkage as a manifestation of the "X-ray tilt," θ_{xr}, defined by eq 1,

$$\theta_{xr} = \arccos(d/d_0) \quad (1)$$

where d_0 is defined as the layer spacing in the "untilted state" and d is the layer spacing in the "tilted state." This expression captures the concept, as illustrated in Figure 1, that the smectic mesogens behave as rods and that tilt of the optic axis corresponds to tilt of these rods through the same angle. In reality, θ_{xr} is typically smaller than θ_{opt} for materials showing a SmA − SmC transition, which is interpreted as resulting from the fact that the core is tilted more than the tails in typical tilted smectics,[12] and the optic axis tilt is dominated by the more polarizable core.

There is very little data in the literature providing measurements of both optical and X-ray tilts as a function of applied electric field for SmA* materials.[13,14] The manifestations of such layer shrinkage are easily seen, however, in the appearance of "quasi-bookshelf" stripes in electroclinic cells when observed between crossed polarizer and analyzer, upon application of a field. These stripes are interpreted as a response of the smectic layers to the shrinkage required by the geometry of the system, forming "horizontal chevron" layer defects.[15]

Electroclinic Effect in de Vries Materials. Most SmA* materials exhibit a relatively small optical tilt with applied field. This result is a combination of a small electroclinic coefficient (tilt/field) and a small saturation tilt. However, recently a class of smectics showing large electroclinic coefficients and large values of the saturation tilt has been discovered. It seems reasonable that such materials would provide a large electromechanical effect. Indeed, such "giant lateral electrostriction" (4% strain at 1.5 V/μm applied field) was reported in an elastomeric SmA* polymer system.[16] In this experiment, the optical thickness, $n * d$ (n = refractive index, d = physical thickness of the sample), of a freely suspended film of aligned SmA* elastomer was measured as a function of field applied parallel to the layers. In the geometry used, the index was expected to remain constant, and the shrinkage of the optical thickness was interpreted as an electromechanical shrinkage of the film thickness d.

Later, however, it was shown that most of the observed change in optical thickness was in the refractive index, not the film thickness, which showed a layer contraction of 1% at 3 V/μm applied field.[17] This apparent disconnect between the observed optical thickness change, and the film thickness change, is due to the fact that the material used in the study[18] belongs to the relatively rare class of de Vries smectics.[5] In the SmA* phase of de Vries smectics, the molecules are tilted, but the tilt direction is random on some length scale small relative to the wavelength of light, giving a kind of

(12) Keller, E. N.; Nachaliel, E.; Davidov, D.; Boffel, C. *Phys. Rev. A* **1986**, *34*, 4363−4369.
(13) Rappaport, A. G.; Williams, P. A.; Thomas, B. N.; Clark, N. A.; Ros, M. B.; Walba, D. M. *Appl. Phys. Lett.* **1995**, *67*, 362−364.
(14) (a) Shashidhar, R.; Naciri, J.; Ratna, B. R. *Adv. Chem. Phys.* **2000**, *113*, 51−76. (b) Spector, M. S.; Heiney, P. A.; Naciri, J.; Weslowski, B. T.; Holt, D. B.; Shashidhar, R. *Phys. Rev. E* **2000**, *61*, 1579−1584.
(15) Skarp, K.; Andersson, G.; Hirai, T.; Yoshizawa, A.; Hiraoka, K.; Takezoe, H.; Fukuda, A. *Jpn. J. Appl. Phys.* **1992**, *31*, 1409−1413.
(16) Lehmann, W.; Skupin, H.; Tolksdorf, C.; Gebhard, E.; Zentel, R.; Kruger, P.; Losche, M.; Kremer, F. *Nature* **2001**, *410*, 447−450.
(17) Kohler, R.; Stannarius, R.; Tolksdorf, C.; Zentel, R. *Appl. Phys. A* **2005**, *80*, 381−388.
(18) Rossle, M.; Zentel, R.; Lagerwall, J. P. F.; Giesselmann, F. *Liq. Cryst.* **2004**, *31*, 883−887.

SmA* phase. Tilting of the optic axis of such phases occurs by ordering of the random tilt, with less than typical layer shrinkage. A perfect de Vries material would show $\theta_{xr} = 0$ in response to any applied electric field, and such materials have recently been discovered.[19] More typically, θ_{xr} is small but non-zero. In the best de Vries SmA* materials, θ_{opt} can be up to 30° in response to fields of ~1 V/μm, with very little layer shrinkage.[14]

Another reported attempt to observe an electromechanical effect based upon the electroclinic effect in SmA* materials failed to detect any strain.[20]

Electroclinic Effect in W317. From the viewpoint of electromechanical materials, the situation is tantalizing but problematic. Large optical tilts are typically accompanied by small layer shrinkage, while materials showing a large ratio θ_{xr}/θ_{opt} (approaching 1, but typically about 0.8−0.9) often have only a small saturation tilt. The mesogen **W317** (structure, phase sequence, and transition temperatures (°C) given below)[21] represents an interesting exception to this generalization.

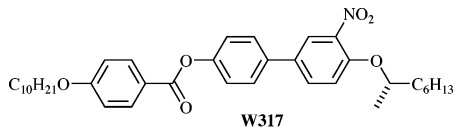

W317

On heating: X — 41 — SmA* — 76 — I
On cooling: X —-7 — SmB_{HEX} — 23 — SmA* — 76 — I

In measurements of θ_{xr} and θ_{opt} as a function of applied electric field in aligned cells, **W317** was found to behave effectively as a rigid rod, with $\theta_{xr} = \theta_{opt}$ over a wide temperature range (27.7−59.6 °C) and with applied fields ranging from 0 to 15 V/μm.[13] For **W317**, $d_0 = 36.09 \pm 0.02$ Å. The tilt observed at 15 V/μm and 27.7 °C was 15°, corresponding to layer spacing of 34.9 Å, or layer shrinkage of 1.2 Å (3.5%). The saturation tilt angle of **W317** at 25 V/μm and 23 °C, measured in another study, is 18.5°, which would correspond to a layer shrinkage of 5.2%.[22] With large stress, such layer shrinkage could, in principle, provide a useful electro-mechanical effect, if it could be coupled with a macroscopic strain.

Main-Chain Poly-W317. To explore this possibility, the synthesis of a main-chain polymeric analogue of **W317**, suitable for eventual conversion to an elastomer, was undertaken. Previous work with smectic mesogens, using metal alkylidene-catalyzed acyclic diene metathesis polymerization (ADMET), demonstrated that main-chain oligomers with excellent mesogenicity and otherwise useful physical properties could be readily obtained.[23] Therefore, the **W317** analogue **10**, possessing double bonds on the ends of the tails, was synthesized as a substrate for ADMET polymerization.

Polymerizations. Grubbs catalysts (1st and 2nd generation) were effective for formation of main-chain polymers **11** from diene **10**. The two catalysts, under various conditions, provided oligomers with a large variation in degree of polymerization. For the high molecular weight materials, the molecular weight distribution was relatively narrow.

For example, polymerization of diene **10** with benzylidene-bis(tricyclohexylphosphine)dichlororuthenium (Grubbs 1st generation catalyst) in dichloroethane (85:1 substrate/catalyst molar ratio) gave an oligomer **11a** with degree of polymerization $n = \sim 10$, according to end group analysis using ^{1}H NMR. Using chlorobenzene as solvent increased the degree of polymerization, reliably affording material with $n = \sim 30$ by end group analysis using ^{1}H NMR.

For these samples, the ratio of trans/cis double bonds in the "tails" of polymers **11** could not be determined directly by NMR. However, 70% trans, 30% cis double bonds have been observed in other, somewhat similar systems.[23a]

As expected, using the 2nd generation Grubbs catalyst, benzylidene[1,3-bis(2,4,6-trimethylphenyl)-2-imidazolidinylidene]dichloro(tricyclohexylphosphine)ruthenium (96:1 substrate/catalyst molar ratio), in combination with chlorobenzene solvent, gave polymer **11b** of much higher molecular weight. No signals corresponding to terminal double bonds could be observed in the ^{1}H NMR spectrum of polymer produced in this way. A rough estimate of the degree of polymerization of these samples was obtained by ^{1}H diffusion ordered spectroscopy (DOSY) in chloroform solvent. An absolute value for the diffusion coefficient of the polymers could not be obtained. However, comparison with **11**, $n = 30$, with typical samples of the higher MW polymers shows the latter have diffusion coefficient $D \sim 1/9$ the value of the former. Since D should be approximately inversely proportional to $n^{1/2}$, the measurements suggest a degree of polymerization $n > 200$ for the samples of **11b** produced using Grubbs 2nd generation catalyst in chlorobenzene.

Polymer Phase Sequence by Polarized Light Microscopy (PLM). Materials obtained by metathesis polymerization of diene **10** were mesogenic, as indicated by PLM and electro-optic behavior in indium tin oxide (ITO)/glass LC cells. In these cells, unaligned samples of polymer could be driven with an applied electric field. All samples of material **11** were found to possess the I − SmA* − SmC* − Glass phase sequence, as shown in Scheme 1. The glass transition temperatures listed indicate the temperatures at which electro-optic activity ceased—all of the materials are glasses at room temperature. Increasing degree of polymerization increases the glass transition temperatures slightly and destabilizes the SmC* phase relative to the SmA*. All of the polymer samples show SmA* phases over at least a 50 °C range. Interestingly, all samples had the same clearing point of 130 °C.

(19) Wand, M. D.; More, K. M.; Thurmes, W. N. Use of germanium FLCs in search of the perfect FLC display. In *Abstracts, 10th International Ferroelectric Liquid Crystal Conference, Stare Jablonki, Poland, 2005*; Institute of Applied Physics and Institute of Chemistry, Military University of Technology: Warsaw, Poland; p O26.
(20) Das, V.; Brown, D. H.; Styring, P.; Allen, R. W. K. *Proc. SPIE-Int. Soc. Opt. Eng.* **2003**, *5051*, 458−563.
(21) Williams, P. A.; Komitov, L.; Rappaport, A. G.; Thomas, B. N.; Clark, N. A.; Walba, D. M.; Day, G. W. *Liq. Cryst.* **1993**, *14*, 1095−1105.
(22) Williams, P. A.; Ros, M. B.; Clark, N. A.; Walba, D. M.; Wand, M. D. *Ferroelectrics* **1991**, *121*, 143−146.
(23) (a) Walba, D. M.; Xiao, L.; Korblova, E.; Keller, P.; Shoemaker, R.; Nakata, M.; Shao, R.; Link, D. R.; Coleman, D. A.; Clark, N. A. *Ferroelectrics* **2004**, *309*, 77−82. (b) Walba, D. M.; Xiao, L.; Keller, P.; Shao, R.; Link, D.; Clark, N. A. *Pure Appl. Chem.* **1999**, *51*, 2117−2123. (c) Walba, D. M.; Keller, P.; Shao, R.; Clark, N. A.; Hillmyer, M.; Grubbs, R. H. *J. Am. Chem. Soc.* **1996**, *118*, 2740−2741.

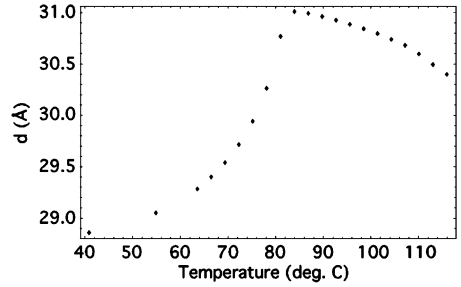

Figure 2. X-ray layer spacing (*d*) as a function of temperature for bulk samples of polymer **11a**, $n \sim 10$.

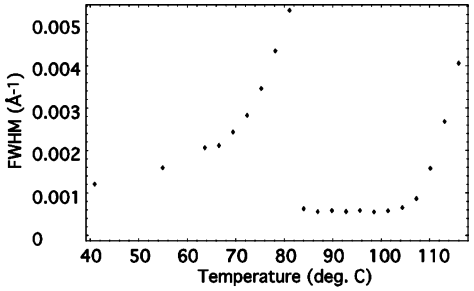

Figure 3. Peak width vs temperature for polymer **11a** ($n \sim 10$).

It is interesting to note that small changes in the **W317** structure change the nature of the SmA* phase dramatically. Thus, while **W317** shows decidedly non de Vries behavior, the incorporation of one double bond in the achiral tail of **W317**, to give **W415** (structure, phase sequence, and transition temperatures (°C) shown below), provides a de Vries SmA* material.[24] This makes the nature of the SmA* phase of polymers **11**, containing double bonds in both tails, difficult to predict from their structure.

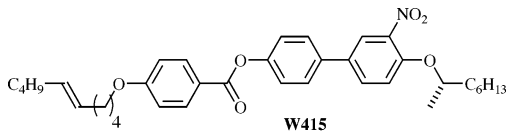

On heating: X — 0.3 — SmC* — 24 — SmA* — 33 — I
On cooling: X — <0 — SmC* — 23 — SmA* — 32 — I

Characterization of Bulk Poly-W317 by Small-Angle X-ray Scattering. The layer spacing as a function of temperature was measured for bulk (powder) samples of polymer **11a** ($n \sim 10$). As shown in Figure 2, the layer shrinkage on progressing from the SmA* phase into the SmC* phase indicates the desired non de Vries behavior for a material with the I − SmA* − SmC* phase sequence, with maximum $\theta_{xr} \sim 21°$ (layer shrinkage ~ 6.8% at saturation in the SmC* phase). Unfortunately, it was not possible in our hands to obtain good data for θ_{opt}, due to difficulties in obtaining well-aligned samples in the SmC* phase.

The full width at half maximum (fwhm) observed for the smectic layer peaks in the SmA* and SmC* phases of polymer **11a** ($n \sim 30$) provide information on the correlation length of the layering in the smectics. Typically, low molar mass smectics give a resolution-limited value of about 5000 Å for the layer correlation length (smectic LCs are quasi-crystalline along the layer normal, due to the finite compressibility of the layers). The polymer samples, however, gave broader peaks than the resolution limit. As shown in Figure 3, the layers in the SmA* phase are poorly defined at the high end of the temperature range and saturate at a value of the fwhm giving a layer correlation length of 3000 Å. This is likely a kinetic effect; it is reasonable that long annealing times in the SmA* temperature range would lead to a resolution-limited correlation length.

At the transition into the SmC* phase, the layers appear to almost "melt" and then reform as the sample is brought further into the SmC* phase. However, the layer structure never becomes as well-defined in the SmC* as in the SmA*, probably due to the increased viscosity of the sample in the SmC* temperature range. Again, this is likely a kinetic effect, though it is unlikely that annealing in the SmC* would ever produce a resolution-limited Bragg peak for the layers. The dramatic change in layer correlation length observed at the SmA* − SmC* transition is interesting, given that the transition appears second order from the gradual increase in θ_{xr} seen on cooling from the SmA* phase.

Fibers Prepared from Poly-W317. All samples of polymers **11** formed smectic LC fibers by pulling from the isotropic melt and then cooling into the LC temperature range. These fibers were stable for many hours in the smectic LC temperature range. For the present work, relatively thick annealed fibers (~200 μm diameter) pulled in the X-ray oven were studied directly in the smectic phases.

As indicated in Figure 4, fibers pulled in the X-ray oven could be rotated about the axis perpendicular to the fiber axis, in the $y-x$ plane, through an angle χ, where $\chi = 0$ when the fiber is oriented along the x axis. The incident X-ray beam wave vector was along z, and the detector was fixed at the Bragg angle in the $y-z$ plane. Measurements of the scattered intensity as a function of χ at $T = 90.4$ °C (in the SmA* phase) are shown in Figure 5. Scattering was observed at $\chi \sim 0°$ and $\chi \sim 90°$. The scattered intensity obtained at $\chi \sim 0°$ was independent of rotation about the long axis of the fiber. A much more intense signal (greater than a factor of 500) was obtained with $\chi \sim 90°$.

As indicated in Figure 5, the data are best interpreted as follows. The fiber is mainly composed of smectic layers oriented normal to the fiber axis (along the polymer main chain). There is, however, a thin sheath of smectic at the fiber−air interface, where the layers are parallel to the air interface (homeotropic alignment). This type of alignment at the smectic−air interface is strongly favored by interfacial free energy terms. Since the scattering from the homeotropic sheath is occurring from the very narrow section of fiber where the layers are normal to y, while the scattering from the core occurs across most of the diameter of the fiber, it is not possible to obtain a good estimate for the thickness of the homeotropic sheath from these data.

(24) (a) Shao, R.-F.; Maclennan, J. E.; Clark, N. A.; Dyer, D. J.; Walba, D. M. *Liq. Cryst.* **2001**, *28*, 117−123. (b) Rudquist, P.; Lagerwall, J. P. F.; Buivydas, M.; Gouda, F.; Lagerwall, S. T.; Clark, N. A.; Maclennan, J. E.; Shao, R.; Coleman, D. A.; Bardon, S.; Bellini, T.; Link, D. R.; Natale, G.; Glaser, M. A.; Walba, D. M.; Wand, M. D.; Chen, X.-H. *J. Mater. Chem.* **1999**, *9*, 1257−1267. (c) Shao, R.-F.; Maclennan, J. E.; Clark, N. A.; Dyer, D. J.; Walba, D. M. *Liq. Cryst.* **2001**, *28*, 117−123.

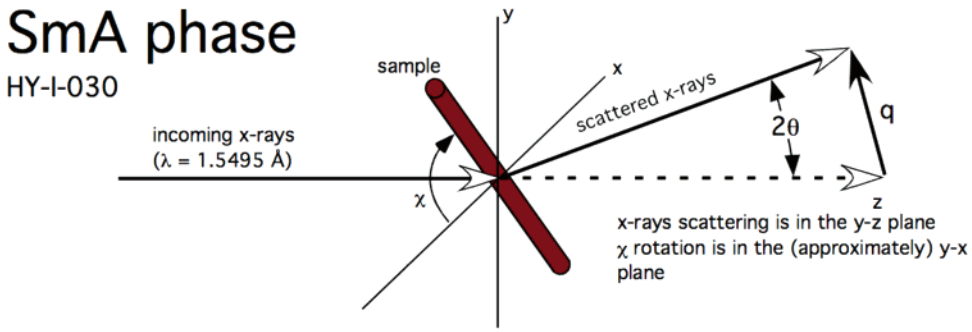

Figure 4. Geometry and definitions used in the small-angle X-ray scattering study of annealed fibers prepared in the X-ray oven.

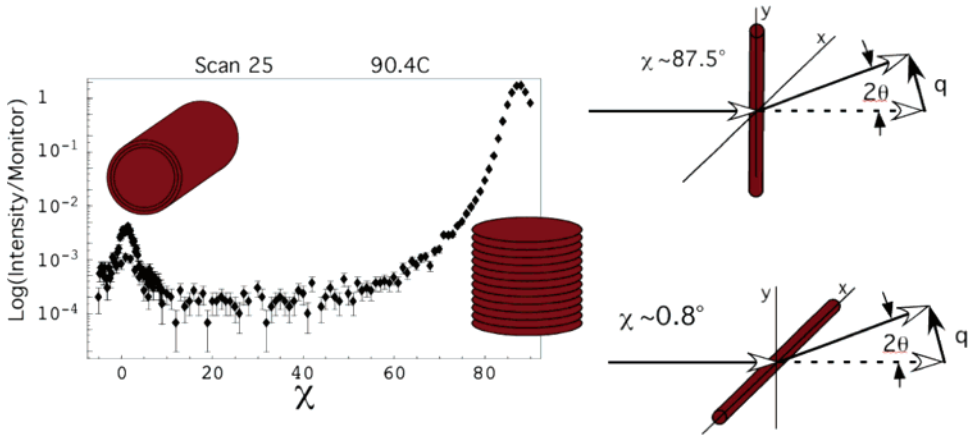

Figure 5. χ scans for an annealed fiber of **11a** ($n \sim 10$) at $T = 90.4$ °C in the SmA* phase. The fibers were first pulled from the isotropic melt and brought to temperature, and data collection was begun immediately and lasted for ~45 min. Data for a scan of χ from ~0° to ~180° is shown. The difference in the scattering intensity at $\chi \sim 0° \sim 180°$ is due to experimental errors in fixing the precise geometry of the system.

χ scans for the region from $\chi = 60°$ to $\chi = 110°$, from the core smectic layers for the SmA* and SmC* phases of an annealed fiber, are given in Figure 6. In a manner similar to the situation in a surface-stabilized FLC (SSFLC) cell, the layers "tilt," forming some kind of chevron defect structure, upon transition from the SmA* to the SmC*. In this annealed fiber, the layer tilt (~12.5° at 62.4 °C) is considerably smaller than θ_{xr} (19° = arccos(d/d_0) = arccos-(29.3/30.9) at 62.4 °C). For chevron SSFLC cells the layer tilt is always smaller than θ_{xr}, but the ratio (θ_{xr}/layer tilt) is typically not as great.

The data shown in Figure 6 are consistent with corrugated layers, somewhat similar to the proposal of Mather for a fiber drawn from the isotropic melt of a main-chain polysilane possessing the I − SmC phase sequence, based upon an analysis of the two-dimensional wide-angle X-ray diffraction pattern (which indicates the orientation of mesogen intermolecular side by side interactions), and the observed θ_{xr} (since this material had no SmA phase, the "untilted" layer spacing was, as is typical, assumed to be the calculated "fully extended molecular length."[25] In that case, the proposed structure has the director along the fiber pulling direction, with the layers tilted by an angle identical to the SmC tilt angle. Alternatively, for the present system the fiber could possess a conical chevron structure.

To differentiate between these possibilities, the X-ray beam was focused to its minimum waist size of 200 μm and scanned across a fiber of diameter 400 μm. The data obtained for $\chi = 74.5°$ and for $\chi = 99.7°$ are given in Figure 7. While the spacial resolution is very poor in this experiment, it can be easily seen that for $\chi = 74.5°$ there is considerably more scattering intensity on the left side of the fiber, while for $\chi = 99.7$, there is more scattering intensity on the right side of the fiber.

This result is not consistent with a corrugated chevron structure, but rather with a conical chevron structure, as indicated in Figure 8. In this structure, the layer shrinkage is accommodated by tilting of the layers to form shallow cones. Stacking of such layers leads to a fiber which would exhibit the behavior seen in the X-ray experiment. In this fiber structure, a line defect runs through the center of the fiber, similar to the planar defect in a chevron SSFLC cell.[26] While such a conical chevron structure seems very attractive, to our knowledge no such structure has been previously reported in the literature.

Electroclinic Effect in Thin Films of Poly-W317. It was not possible to obtain data speaking to the electroclinic coefficient, or layer shrinkage with director tilt, for unaligned samples of polymer **11**, and conventional methods for LC alignment (shearing, rubbed polymer alignment layers) proved ineffective for these materials. Well-aligned thin films could be obtained, however, by taking advantage of the rheological properties described above. Specifically, polymer glass fibers could be easily fabricated from the isotropic melt of all samples of polymer **11**. A sample of polymer was

(25) Rousseau, I. A.; Qin, H. H.; Mather, P. T. *Macromolecules* **2005**, *38*, 4103−4113.
(26) (a) Rieker, T. P.; Clark, N. A.; Smith, G. S.; Parmar, D. S.; Sirota, E. B.; Safinya, C. R. *Phys. Rev. Lett.* **1987**, *59*, 2658−61. (b) Clark, N. A.; Rieker, T. P. *Phys. Rev. A* **1988**, *37*, 1053−1056.

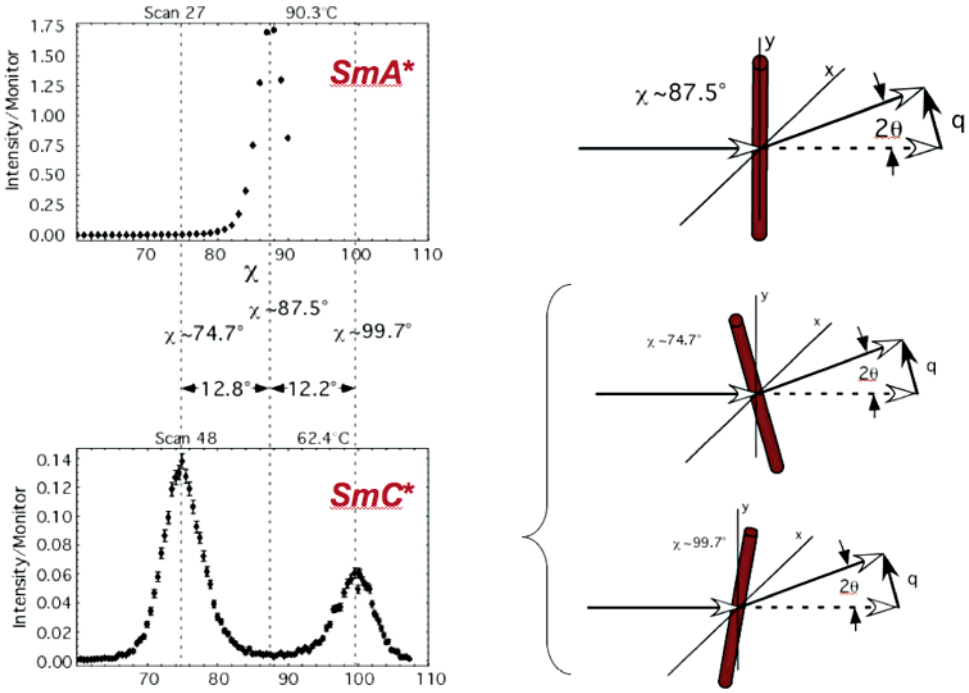

Figure 6. χ scans for an annealed fiber of **11a** ($n \sim 10$) at 90.3 °C (SmA*) and 62.4 °C (SmC*). The difference in the scattering intensity at $\chi \sim 74.4°$ and $\chi \sim 99.7°$ is due to experimental errors in fixing the precise geometry of the system.

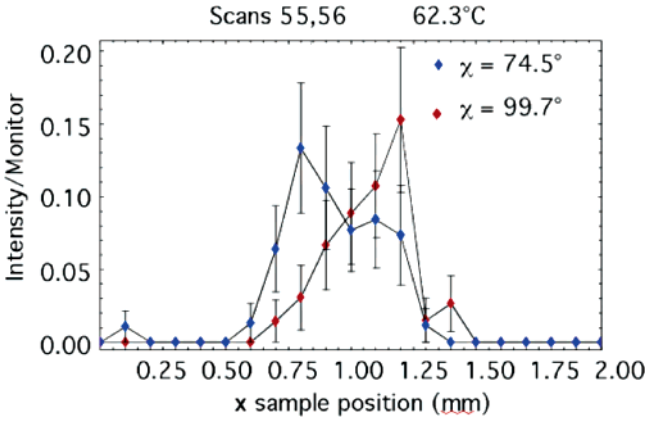

Figure 7. Lateral scan of a fiber of **11a** ($n \sim 10$) at two different values of χ. The beam spot diameter is 200 μm, and the fiber diameter is 400 μm. The sample position (x) is measured for the center of the beam, relative to the center of the fiber, defined as $x = 1.00$ mm (i.e., the beam no longer hits the fiber at $x = 0.40$ and $x = 1.60$.

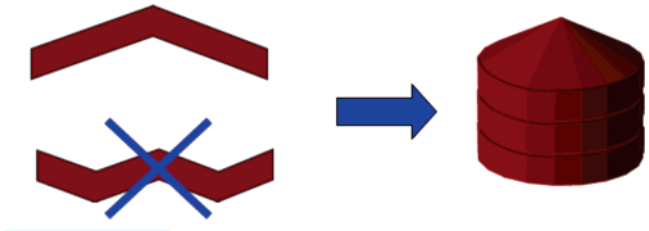

Figure 8. Conical chevron structure indicated by the X-ray data.

placed in a small indentation drilled into a piece of glass. The polymer was melted into the isotropic phase by placing the glass holder on a hot plate at $T > T_{SmA-I}$. A micropipet was typically used to pull fibers directly into the ambient lab environment. The glass tip was contacted with the cleared polymer and then raised by hand to produce long smectic glass fibers. The diameter of such fibers typically ranged from 10 to 100 μm and could be controlled to some extent by varying the pulling velocity. Under these primitive conditions, it was easier to pull long fibers from the lower molecular weight polymers **11a**, but samples of **11b** also provided these "quenched" fibers.

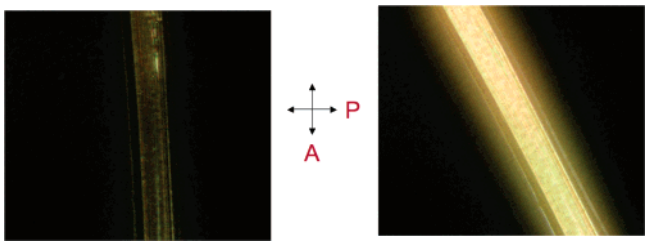

Figure 9. Photomicrographs of a glass fiber of polymer **11a** ($n \sim 10$) at room temperature observed between crossed analyzer (vertical) and polarizer. The fiber diameter is ~20 μm. While the optical properties of the fibers observed in this way are complicated, the data are clearly consistent with a conical chevron layer structure.

As indicated in Figure 9, glass fibers of **11a** ($n \sim 10$) show excellent extinction when the fiber axis is parallel or perpendicular to the polarizer. Rotation of the fibers by 45° from extinction maximizes the transmission. This behavior is consistent with a fiber structure similar to that seen in the annealed fibers, where the homeotropic sheath, if there is one, is thin relative to the fiber diameter. While texture is observable within the fibers, the uniformity of the alignment is qualitatively excellent.

To obtain electro-optic data on aligned samples of **11**, a new method for preparation of smectic thin films has been developed, starting from smectic glass fibers. This method, which is illustrated in Figure 10, involves the following steps: (1) Place an aligned glass fiber sample between solid substrates with appropriate spacers. (2) With an appropriate mass placed on the top substrate, heat the system rapidly into the SmA* phase using a hot plate. (3) Wait until the

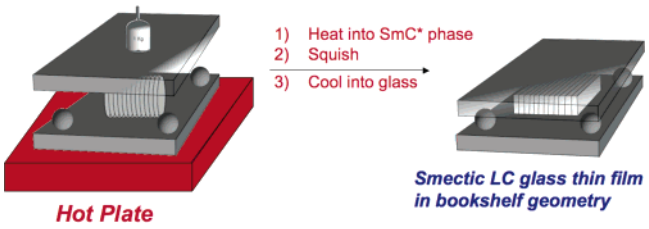

Figure 10. Method for producing smectic thin films in the "bookshelf" geometry, from polymer fibers.

cell collapses onto the spacers. With use of polymer **11a** ($n \sim 10$), such a cell was prepared with a 7.5 μm cell gap, using Mylar spacers (the mass was a 1 kg weight). Due to the large anisotropy in the shear viscosity in smectics, this process leaves the smectic layer structure in tact and simply changes the geometry of the sample from cylindrical to rectangular while maintaining the volume of the sample. The cell could be allowed to cool to room temperature and then heated once back into the SmA* phase without large degradation of the alignment. However, repeated heating and cooling cycles did cause damage to the alignment, visible by polarized light microscopy, and it was not possible to determine θ_{opt} in the SmC* phase of the samples due to the presence of alignment defects in the SmC* phase.

Such cells, heated into the SmA* phase, can be driven by an applied electric field using ITO electrodes coated onto the substrate inner surfaces. The behavior of these cells is precisely as expected for the proposed structure. Thus, in the first few switching events, a large electroclinic θ_{opt} of ca. $\pm 23°$ (close to the bulk θ_{xr} of 21°) could be observed in the polarized light microscope, in response to an applied electric field of 12 V/μm, at ~82 °C (just above the transition into the SmC* phase). However, after repeated switching, the alignment degraded substantially, such that it was no longer possible to measure the electroclinic tilt angle. In the context of electromechanical materials this behavior is promising since the misalignment is almost certainly to be due to substantial layer shrinkage with director tilt in a non de Vries material.

Conclusions

The synthesis and some properties of a new main-chain chiral smectic LC polymer system, prepared by ADMET polymerization of an α,ω-unsaturated mesogen, is described. The new materials are shown to exhibit layer shrinkage at the SmA* − SmC* transition and also to possess a large electroclinic effect in the SmA* phase close to the SmC* transition. Elastomers based upon this system are of potential utility as electromechanically active materials. Methods for cross-linking of the polymer chains and elucidation of the properties of elastomers derived from this basic strategy are under investigation.

Acknowledgment. We thank the Liquid Crystal Materials Research Center (NSF MRSEC Award No. DMR-0213918) for financial support of this work.

CM0606373